

Charge-symmetry violation in pion scattering from three-body nuclei

A. E. Kudryavtsev* and V. E. Tarasov†

Institute for Theoretical and Experimental Physics, 25 Bolshaya Chermushkinskaya Street, Moscow RU-117259, Russia

B. L. Berman,‡ W. J. Briscoe,§ K. S. Dhuga,|| and I. I. Strakovsky¶

Center for Nuclear Studies, Department of Physics, The George Washington University, Washington, D.C. 20052

(Received 22 April 2002; published 27 November 2002)

We discuss the experimental and theoretical status of charge-symmetry violation (CSV) in the elastic scattering of π^+ and π^- on ^3H and ^3He . Analysis of the experimental data for the ratios r_1 , r_2 , and R at $T_\pi = 142, 180, 220,$ and 256 MeV provides evidence for the presence of CSV. We describe pion scattering from the three-nucleon system in terms of single- and double-scattering amplitudes. External and internal Coulomb interactions as well as the Δ_{33} -mass splitting are taken into account as sources of CSV. Reasonable agreement between our theoretical calculations and the experimental data is obtained for $T_\pi = 180, 220,$ and 256 MeV. For these energies, it is found that the Δ_{33} -mass splitting and the internal Coulomb interaction are the most important contributions for CSV in the three-nucleon system. The CSV effects are rather sensitive to the choice of pion-nuclear scattering mechanisms, but at the same time, our theoretical predictions are much less sensitive to the choice of the nuclear wave function. It is found, however, that data for r_2 and R at $T_\pi = 142$ MeV do not agree with the predictions of our model, which may indicate that there are additional mechanisms for CSV which are important only at lower energies.

DOI: 10.1103/PhysRevC.66.054007

PACS number(s): 25.45.De, 25.80.Dj, 24.80.+y, 25.10.+s

I. INTRODUCTION

The issue of charge-symmetry violation (CSV) is fundamental to our understanding of hadronic interactions, and many experimental and theoretical studies have addressed this issue (see review, Ref. [1]). In the framework of QCD, CSV arises from the mass difference between the u and d quarks. The other principal cause for CSV comes from the electromagnetic interaction.

Weinberg [2] pointed out that the effective chiral πN Lagrangian, coming from QCD, contains a term which violates charge symmetry (see, also, a recent review by Meissner [3]). Thus, not only are there kinematic reasons for CSV due to the mass differences within baryon multiplets, but direct CSV effects should exist as well. Recently, Gashi *et al.* [4] analyzed low-energy πN scattering data, and found some indications for direct CSV effects in the strong-interaction sector.

Another way to study CSV is through the pion-nuclear interaction in the lightest nuclei, particularly via isomirror elastic scattering. For the deuteron case, the π^+d cross section is compared with that for π^-d in Masterson *et al.* [5] and Baru *et al.* [6], but only small differences are found.

For pion elastic scattering from ^3H and ^3He , one can consider three mirror ratios formed from the differential cross sections:

$$r_1 = \frac{d\sigma/d\Omega(\pi^+{}^3\text{H})}{d\sigma/d\Omega(\pi^-{}^3\text{He})},$$

$$r_2 = \frac{d\sigma/d\Omega(\pi^-{}^3\text{H})}{d\sigma/d\Omega(\pi^+{}^3\text{He})},$$

$$R = r_1 \cdot r_2, \quad (1)$$

where R is referred to as the ‘‘superratio’’ [7]. The $\pi^+{}^3\text{H}$ and $\pi^-{}^3\text{He}$ scattering cross sections are isomirror ones, as are $\pi^-{}^3\text{H}$ and $\pi^+{}^3\text{He}$. If charge symmetry were conserved, all three ratios would be equal to unity. Of course, the Coulomb interaction is not charge symmetric and has to be taken into account.

The experimental study of these ratios has been concentrated on large-angle scattering [everywhere below all angles are quoted in the center of mass (c.m.)] because the Coulomb interaction, which intrinsically violates charge symmetry, makes a significant contribution in the forward-scattering region. In a series of LAMPF experiments [7–10], the ratios (1) were measured in the range of the $\Delta_{33}(1232)$ πN resonance. Significant deviation (several standard deviations) from unity (up to $\sim 20\%$) was observed for r_2 and R in the angular range outside of the Coulomb cone, $\theta \gtrsim 30^\circ$. In addition, strong angular dependence of both r_2 and R was ob-

*Email address: kudryavt@heron.itep.ru

†Email address: tarasov@vitep5.itep.ru

‡Email address: berman@gwu.edu

§Email address: briscoe@gwu.edu

||Email address: dhuga@gwu.edu

¶Email address: igor@gwu.edu

served in the angular interval between $\theta \approx 60^\circ$ and 90° . These CSV effects are much more pronounced for ${}^3\text{H}$ and ${}^3\text{He}$ than for ${}^2\text{H}$, where the observed asymmetry A_π ¹ is not nearly as large: it is only about 2% (see, for example, Ref. [5]). In addition, inelastic-scattering data for the ratios (1) at excitation energy below 20 MeV have been reported in Ref. [11], and elastic differential cross sections at back angles in Ref. [12].

Thus, CSV effects manifest themselves clearly in the three-nucleon system, even if they are very small in the deuteron case. For this reason, the main goal of our theoretical analysis is the elucidation of the mechanisms that enhance CSV in the three-nucleon system. In other words, can the observed enhancement be due only to the well-known mass differences of the hadron multiplets together with the Coulomb interaction? Previous studies have indicated that the main reason for CSV in the case of the deuteron is the mass difference of the charge $\Delta_{33}(1232)$ -isobar states. The influence of this effect on the scattering amplitude of the πd elastic scattering was discussed in the papers by Masterson *et al.* [5] and Baru *et al.* [6] for single and single-with-double scattering, respectively. Naturally, as the number of multiple-scattering diagrams increases with an increasing number of nucleons, one expects the effect of the Δ_{33} -mass splitting to be more prominent for ${}^3\text{H}$ and ${}^3\text{He}$ than for ${}^2\text{H}$.

In addition to the interaction between charged pions and nuclei due to the external Coulomb force, there is an internal Coulomb interaction due to the difference in the wave functions (WFs) of ${}^3\text{H}$ and ${}^3\text{He}$. (Note that in terms of the strong interaction, there is no difference between the WFs of ${}^3\text{H}$ and ${}^3\text{He}$.) One difference in these WFs arises from the additional Coulomb repulsion between the two protons in ${}^3\text{He}$, which is not present in ${}^3\text{H}$.

In Ref. [13], the difference in the structure of ${}^3\text{H}$ and ${}^3\text{He}$ has been described by a first order optical potential in the pion-nuclear interaction in which the ${}^3\text{H}$ and ${}^3\text{He}$ charge and magnetic form factors extracted from experimental data on elastic electron scattering from ${}^3\text{H}$ and ${}^3\text{He}$ were used. A more detailed analysis of pion- ${}^3\text{H}/{}^3\text{He}$ elastic and inelastic scattering was reported in Ref. [14], where an optical single-scattering pion-nuclear potential, calculated at a microscopic level with a realistic three-nucleon wave function, was used. No reasonable description of the CSV effects was achieved when the calculations were performed with isospin-

¹Historically, the CSV experimental data for $\pi^\pm d$ elastic scattering have been evaluated in terms of the asymmetry A_π :

$$A_\pi = \frac{d\sigma/d\Omega(\pi^- d) - d\sigma/d\Omega(\pi^+ d)}{d\sigma/d\Omega(\pi^- d) + d\sigma/d\Omega(\pi^+ d)}.$$

If we define r_d by analogy with the ratios (1), we get

$$r_d = \frac{d\sigma/d\Omega(\pi^- d)}{d\sigma/d\Omega(\pi^+ d)} = 1 + \epsilon,$$

and for small ϵ we have $A_\pi = \epsilon/2$. Thus, $r_d \approx 1 + 2A_\pi$.

symmetric wave functions for both nuclei. A different approach was used in Ref. [15], where the difference in the WFs of ${}^3\text{H}$ and ${}^3\text{He}$ was taken into account explicitly. In all of these approaches [13–15], the difference in the structure of the three-nucleon system results in a sharp enhancement of the ratios r_2 and R in the angular range $60^\circ \leq \theta \leq 90^\circ$.

One of the reasons for this behavior of the angular distribution is that the elastic differential cross section in the single-scattering approach contains a significant contribution at small scattering angles and has a minimum at $\theta \approx 90^\circ$ which is related to the dip in the πN non-spin-flip amplitude. Therefore, even a small contribution to the interaction that violates charge symmetry (e.g., the Coulomb interaction) can produce an enhanced effect. The influence of the Δ_{33} -mass splitting on the observed CSV effect might also result in a large effect in this angular range.

Moreover, to understand the angular distribution in detail, one must look beyond the single-scattering approach to the πN interaction. We therefore examine the contributions of both single- and double- πN scattering to the pion-nuclear scattering amplitude following techniques developed in Ref. [6]. We then take CSV effects into account to obtain expressions for the ratios (1), which are then compared with the experimental data [7–10].

An analysis of the experimental status for the ratios (1) at energies spanning the Δ_{33} resonance is given in Sec. II. In Sec. III, we explain how the basic ingredients of the scattering amplitude and the constraints of single and double scattering are combined for $\pi^3\text{H}$ and $\pi^3\text{He}$ elastic scattering. In Sec. IV, we derive expressions for the scattering amplitudes, taking into account all three effects responsible for CSV. In Sec. V, we discuss the influence of these factors on the ratios (1) to show the effect of the individual CSV factors, and we compare the results of our calculations with the data. In Sec. VI, we discuss some related issues associated with CSV effects in other nuclei over broader ranges in energy and scattering angle. In Sec. VII, we summarize our findings.

II. ANALYSIS OF THE EXPERIMENTAL STATUS

CSV in pion-nucleus scattering was first claimed to have been observed in the difference of total $\pi^\pm d$ cross sections measured at PSI [16], and ascribed to the Δ_{33} -mass splitting. Essentially, the total cross section is mainly determined by the forward-scattering amplitude, which at small angles can be approximated well by single scattering. In this approach, the different charge states of the Δ_{33} are excited in π^+ and π^- scattering on the deuteron, and the result is the small observed CSV effect. This has been discussed widely (see e.g., the book by Ericson and Weise [17]). The situation with the observation of CSV effects in the $\pi^\pm d$ differential cross sections is less clear. The first systematic study of the CSV effect in the differential $\pi^\pm d$ cross sections was done at LAMPF [5]. There have been several subsequent measurements at LAMPF and TRIUMF for both $\pi^+ d$ and $\pi^- d$ (see Ref. [6] for details). The experimental data weakly suggest a small effect in the asymmetry A_π for the deuteron. For example, in Ref. [5], an asymmetry $A_\pi \approx 2\%$ at 143 MeV near 90° in the c.m. frame is reported. However, Smith *et al.* [18],

in an independent measurement done at TRIUMF, reported asymmetries of $-1.5 \pm 0.6\%$ at back angles and various energies. Thus, the magnitude of CSV is at most 1%–2%, the sign is uncertain, and the experimental uncertainties are only slightly less than the A_π values themselves.

At about the same time, however, measurements of the ratios (1) for ${}^3\text{H}$ and ${}^3\text{He}$ at LAMPF obtained significantly larger effects. The first evidence for a sizable CSV in the differential $\pi^\pm {}^3\text{H}/{}^3\text{He}$ cross sections² below and at the Δ_{33} resonance was seen for the range of c.m. scattering angles between 45° and 95° [7]. The effect seems to peak near 80° in the c.m. frame (e.g., $r_2 \approx R \approx 1.2$ at 180 MeV [7]). The experiment was repeated with better statistics and systematics for approximately the same range of scattering angles at energies spanning the Δ_{33} [8] and beyond [9]. These measurements also were extended to backward angles from 120° to 170° [19] and are reported in the previous paper [10]. The experimental data for all three ratios (1) for incident pion energies between 142 and 256 MeV are shown in Fig. 1 of the associated paper by Briscoe *et al.* [10]. The agreement between the four data sets, on the whole, is very good. The bump observed at $\sim 80^\circ$, corresponding to the minimum in the non-spin-flip amplitude, is obvious in the ratios r_2 and R for 142 and 180 MeV (below and on the Δ_{33} resonance). Thus, CSV effects in $\pi^3\text{H}$ and $\pi^3\text{He}$ scattering are large and statistically significant. The main goal of the present work is to provide a theoretical basis for these large effects in the three-nucleon system.

III. AMPLITUDES OF PION ELASTIC SCATTERING FROM ${}^3\text{H}$ AND ${}^3\text{He}$

We formulate the pion-nuclear amplitude in the range of the Δ_{33} resonance as a combination of a single- and double-scattering of pions from the nucleons in the nucleus. For the $A=3$ nuclei, the appropriate diagrams are shown in Fig. 1. The elementary πN amplitude $\hat{f}_{\pi N}$ is taken as the P_{33} partial wave, as if πN scattering takes place entirely through the Δ_{33} resonance:

$$\hat{f}_{\pi N} = f_{P_{33}} \cdot \hat{S} \cdot \hat{T}, \quad (2)$$

where

$$f_{P_{33}} = \frac{1}{2ik_{cm}} [e^{2i\delta_{33}(k)} - 1],$$

and \hat{S} and \hat{T} are the spin and isospin projection operators for the πN system for total spin 3/2 and isospin 3/2:

$$\hat{S} = 2(\hat{k}_1 \cdot \hat{k}_2) + i \vec{\sigma} \cdot [\hat{k}_1 \times \hat{k}_2], \quad \hat{T} = \frac{1}{3}(2 + \vec{t} \cdot \vec{\tau}). \quad (3)$$

²To eliminate some systematic uncertainties, normalized yields were used for the experimental determination of the ratios (1).

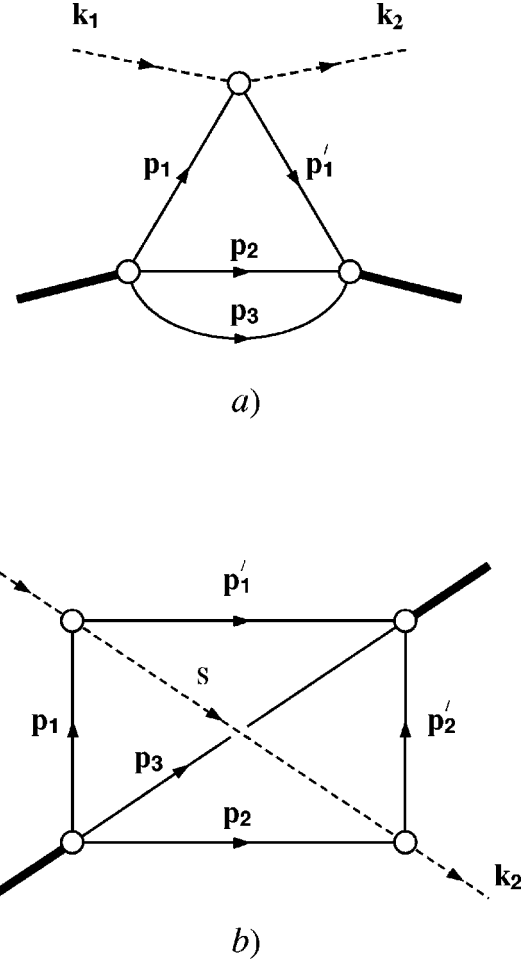


FIG. 1. (a) Single- and (b) double-scattering diagrams used in the present calculations for $\pi^\pm {}^3\text{H}/{}^3\text{He}$ elastic scattering.

Here, \vec{t} and $\vec{\tau}/2$ are the isospin operators of the pion and nucleon, respectively, $\vec{\sigma}$ and $\vec{\tau}$ are Pauli matrices, \hat{k}_1 and \hat{k}_2 are the unit vectors in the direction of the incoming and outgoing pions in the c.m. frame, respectively, and \vec{k}_{cm} is the pion momentum in the c.m. frame. Everywhere below, we use the following notation:

$$\hat{S} = a + \hat{b}, \quad a = 2(\hat{k}_1 \cdot \hat{k}_2), \quad \hat{b} = (\vec{\sigma} \cdot \vec{b}), \quad \vec{b} = i[\hat{k}_1 \times \hat{k}_2]. \quad (4)$$

The WF of the ${}^3\text{H}$ and ${}^3\text{He}$ can be written as

$$\Psi = \psi(\vec{r}_1, \vec{r}_2, \vec{r}_3) \sum_{i=1}^3 X_i \cdot Y_i, \quad (5)$$

where X_i and Y_i correspond to the spin and isospin parts of the WF, respectively,

$$X_i = \frac{1}{\sqrt{2}}(\chi_i^+ \chi)(\chi_j^+ \sigma_2 \chi_k^*), \quad Y_i = \frac{1}{\sqrt{6}}(\eta_i^+ \vec{\tau} \eta)(\eta_j^+ \vec{\tau} \eta_k^*), \quad (6)$$

where χ and η are the spinor and isospinor of the nucleus, respectively, and χ_i , χ_j , and χ_k (η_i , η_j , η_k) are the spinors (isospinors) of the nucleons of the nucleus (i, j , and k are cyclic). Equations (6) represent states of pairs of nucleons (jk) such that their total spin $S=0$ and their isospin $T=1$. The representation (5) for the WFs of ${}^3\text{H}$ and ${}^3\text{He}$ can be generalized for more complicated wave configurations of nuclei, as is discussed in Ref. [20].

The coordinate part of the WF is taken into account in a symmetric form corresponding to a simple S -shell model. In the following calculations, we use two different forms of the radial WF:

(i) The simple Gaussian form

$$\psi(\vec{r}_1, \vec{r}_2, \vec{r}_3) \sim \exp\left[-\frac{1}{2b^2} \sum_{i=1}^3 (\vec{r}_i - \vec{r}R_0)^2\right], \quad (7)$$

where $b=1.65$ fm and $\vec{R}_0 = \frac{1}{3}(\vec{r}_1 + \vec{r}_2 + \vec{r}_3)$, taken from Kamalov *et al.* [14]. The slope $b=1.65$ fm was chosen in Ref. [14] by a best fit to the experimental data for the ${}^3\text{H}$ charge form factor below momentum transfer $Q=400$ MeV/c [21]. This form of the WF fails to reproduce the minimum of the charge form factor at $Q \approx 710$ MeV/c, however, the elastic $\pi^{\pm 3}\text{He}$ differential cross sections are reproduced well at $T_\pi=100$ and 200 MeV, and at backward-scattering angles, the results of the calculations with the WF (7) tend toward the suppression seen in the experimental cross sections [14].

(ii) The two-component Gaussian parametrization

$$\psi(\vec{r}_1, \vec{r}_2, \vec{r}_3) = N \sum_{m=1}^2 D_m \exp\left[-\frac{\alpha_m}{2} \sum_{i=1}^3 (\vec{r}_i - \vec{R}_0)^2\right], \quad (8)$$

where $D_1=1$, $D_2=-1.9$, $\alpha_1=0.70$ fm $^{-2}$, $\alpha_2=2.24$ fm $^{-2}$, and N is a normalization constant given in Appendix A. This WF was successfully used by Foursat *et al.* [22] for the description of the differential cross sections for the reaction ${}^4\text{He}(p, d){}^3\text{He}$ at 770 MeV for a wide range of scattering angles. The WF (8) reproduces the minimum of the ${}^3\text{He}$ charge form factor at $Q=670$ MeV/c, but is larger than the experimental data at momentum transfer $Q \approx 300 - 400$ MeV/c.

A. Single-scattering approximation

The diagram in Fig. 1(a) corresponds to the single-scattering approximation for the elastic pion-nuclear scattering amplitude. To calculate this amplitude, we need to compute the matrix element for the operator (2) between initial- and final-state wave functions. We neglect both the Fermi motion of the nucleon inside the nucleus and the off-shell corrections to the πN amplitudes in expression (2). (We discuss the accuracy of both of these approximations in Sec. VI B.) Taking nuclear WFs in the form (5), we exclude spin

and isospin variables of the nucleons. As in Ref. [20], the single-scattering amplitude \hat{F}_1 is

$$\hat{F}_1 = F(\vec{\Delta}) f_{P_{33}} \hat{\Lambda}_1, \quad (9)$$

where $F(\vec{\Delta})$ is a nuclear form factor defined by Eq. (A4) and $\vec{\Delta}$ is the three-momentum transfer. The operator $\hat{\Lambda}_1$ acts on the nuclear spin and isospin variables and is expressed as

$$\hat{\Lambda}_1 = \frac{1}{3}[(6 + \vec{t} \cdot \vec{\tau})a + (2 - \vec{t} \cdot \vec{\tau})\hat{b}], \quad (10)$$

where a and \hat{b} have been defined in Eq. (4). Calculating the matrix element from the operator $\hat{\Lambda}_1$ on isotopic variables, we get

$$\hat{\Lambda}_1 = \begin{cases} \frac{1}{3}(7a + \hat{b}) & \text{for } \pi^+{}^3\text{He} \text{ and } \pi^-{}^3\text{H} \text{ scattering,} \\ \frac{1}{3}(5a + 3\hat{b}) & \text{for } \pi^+{}^3\text{H} \text{ and } \pi^-{}^3\text{He} \text{ scattering.} \end{cases} \quad (11)$$

In terms of $\hat{\Lambda}_1$, the expression for the differential cross section with unpolarized particles yields

$$\frac{d\sigma}{d\Omega} = F^2(\vec{\Delta}) |f_{P_{33}}(k)|^2 \frac{1}{2} \text{Tr}\{\hat{\Lambda}_1^+ \hat{\Lambda}_1\}, \quad (12)$$

where

$$\begin{aligned} & \frac{1}{2} \text{Tr}\{\hat{\Lambda}_1^+ \hat{\Lambda}_1\} \\ &= \begin{cases} \frac{1}{9}(1 + 195z^2) & \text{for } \pi^+{}^3\text{He} \text{ and } \pi^-{}^3\text{H} \text{ scattering,} \\ \frac{1}{9}(9 + 91z^2) & \text{for } \pi^+{}^3\text{H} \text{ and } \pi^-{}^3\text{He} \text{ scattering,} \end{cases} \end{aligned} \quad (13)$$

where $z = (\hat{k}_1 \cdot \hat{k}_2) = \cos \theta$. In addition to a lower form factor $F(\vec{\Delta})$, the angular dependence of $d\sigma/d\Omega$ is determined by the factors of Eq. (13). Expressions (12) and (13) show that $d\sigma/d\Omega$ is suppressed at $z=0$ ($\theta=90^\circ$), where only the spin-flip πN amplitude contributes. Thus, for the $A=3$ case, there is a more significant spin-flip suppression than for the deuteron case, where (see, for example, Ref. [6])

$$\frac{d\sigma_{\pi d}}{d\Omega} \sim (1 + 5z^2)$$

and the minimum in the cross section is much weaker. We note that this kind of suppression of the spin-flip πN amplitude in the single-scattering term for the ${}^3\text{H}/{}^3\text{He}$ case was pointed out in Ref. [7], following Ref. [23].

In Figs. 2–5, the single-scattering contributions to the differential cross sections for incident pion kinetic energies

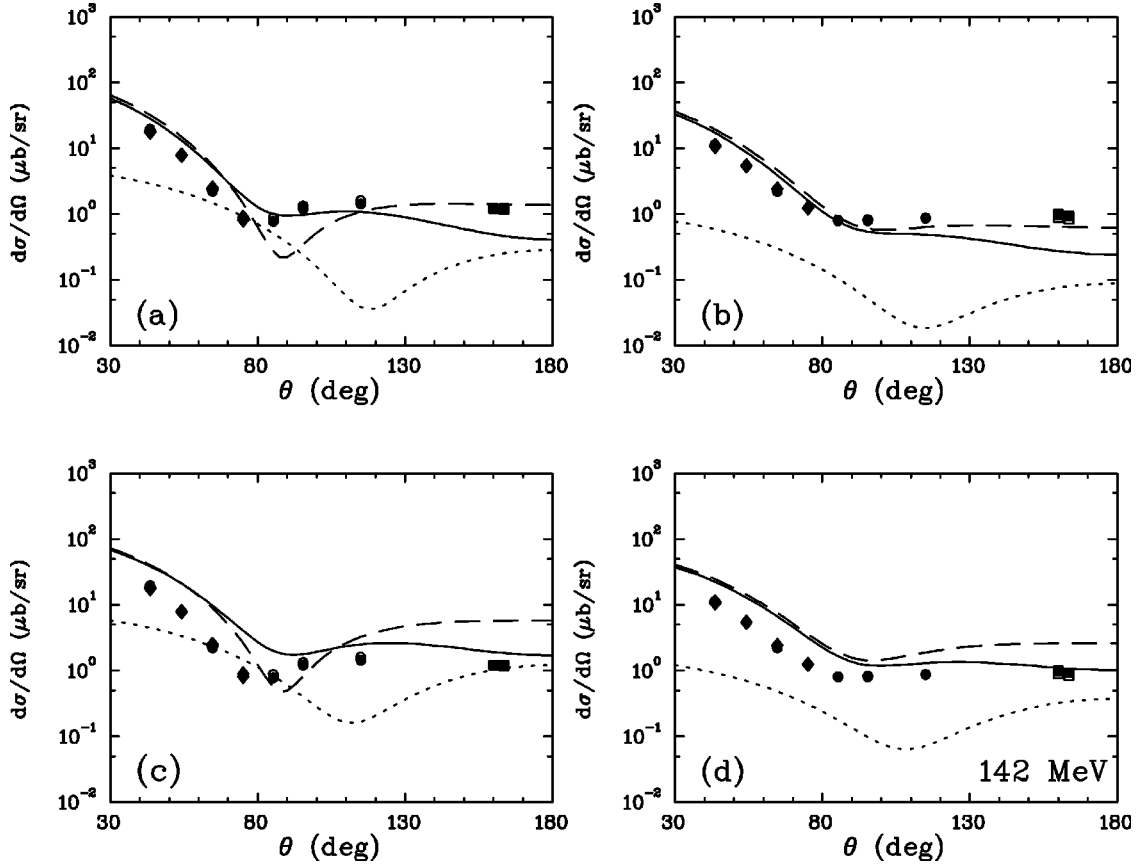


FIG. 2. Differential cross sections for $\pi^{\pm 3}\text{He}/^3\text{He}$ elastic scattering for $T_{\pi}=142$ MeV. Plotted are results for (a) and (b) WFs (7) and (c) and (d) WF (8). Experimental data are from Refs. [7] (diamonds), [8] (circles), [9] (triangles), and [10] (squares), with $\pi^{+3}\text{He}/^3\text{H}$ (filled symbols) and $\pi^{-3}\text{He}/^3\text{H}$ (open symbols). The cross sections (a) and (c) are for $\pi^{+3}\text{He}$ and $\pi^{-3}\text{H}$ and (b) and (d) for $\pi^{+3}\text{H}$ and $\pi^{-3}\text{He}$. The solid curves give the total contribution. Results for single and double scattering alone are shown by the dashed and dotted curves, respectively.

$T_{\pi}=142, 180, 220,$ and 256 MeV, for both versions of the radial part of the WFs (7) and (8), are shown by the dashed curves.

B. Double-scattering approximation

Let us consider the double-scattering amplitude \hat{F}_2 , such as in Ref. [20], corresponding to the diagram shown in Fig. 1(b). (Calculations of double-spin-flip amplitudes were performed recently [24].) In the same approximation as was used while calculating the single-scattering term,

$$\hat{F}_2 = 4\pi \frac{9}{2} f_{P_{33}}^2 \int \frac{d^3\vec{q}}{(2\pi)^3} \frac{d^3\vec{Q}}{(2\pi)^3} \frac{d^3\vec{Q}'}{(2\pi)^3} \times \varphi(\vec{q}', \vec{Q}') \varphi(\vec{q}, \vec{Q}) G_{\pi} \hat{\Lambda}_2, \quad (14)$$

where the WF in the momentum space operator $\varphi(\vec{q}, \vec{Q})$ is defined by Eq. (A2). The momenta \vec{q} , \vec{Q} , \vec{Q}' , and \vec{q}' relate to the momenta \vec{p}_i and \vec{p}'_i , shown in Fig. 1(b), via $\vec{q}=(\vec{p}_2 - \vec{p}_3)/2$, $\vec{Q}=(\vec{p}_2 + \vec{p}_3 - \vec{p}_1)/3$, $\vec{Q}'=(\vec{p}'_2 + \vec{p}_3 - \vec{p}'_1)/3$, and $\vec{q}'=\vec{q} - \frac{1}{2}\vec{Q} + \frac{1}{2}\vec{Q}' + \frac{1}{3}\vec{\Delta}$. In Eq. (14), G_{π} is the Green's

function for the intermediate state, which, neglecting kinetic energy of the intermediate nucleons, has the form

$$G_{\pi}=(k_1^2 - \vec{s}^2 + i0)^{-1}, \quad (15)$$

where $\vec{s}=\vec{k}_1 - \vec{Q} + \vec{Q}' - \frac{1}{3}\vec{\Delta}$. By analogy with Eq. (4), we introduce a_i and \hat{b}_i , where $i=1,2$, for the first and second nucleons:

$$a_{1,2}=2(\hat{k}_{1,2} \cdot \hat{s}), \quad \hat{b}_{1,2}=(\vec{\sigma} \cdot \vec{b}_{1,2}), \quad (16)$$

where $\vec{b}_1=i[\hat{k}_1 \times \hat{s}]$, $\vec{b}_2=i[\hat{s} \times \hat{k}_2]$, and $\hat{s}=\vec{s}/|\vec{s}|$. The operator $\hat{\Lambda}_2$ then can be written as

$$\hat{\Lambda}_2 = \frac{4}{9}(5 + \vec{t} \cdot \vec{\tau})a_1a_2 + \frac{4}{9}(a_1\hat{b}_2 + a_2\hat{b}_1) - \frac{1}{9}(6 + 3\vec{t} \cdot \vec{\tau})\hat{b}_1\hat{b}_2 - \frac{1}{9}(6 + 5\vec{t} \cdot \vec{\tau})\hat{b}_2\hat{b}_1. \quad (17)$$

The operator $\hat{\Lambda}_2$ depends explicitly on the spin and isospin variables of the nuclei and the pion. $\hat{\Lambda}_2$ also depends on the

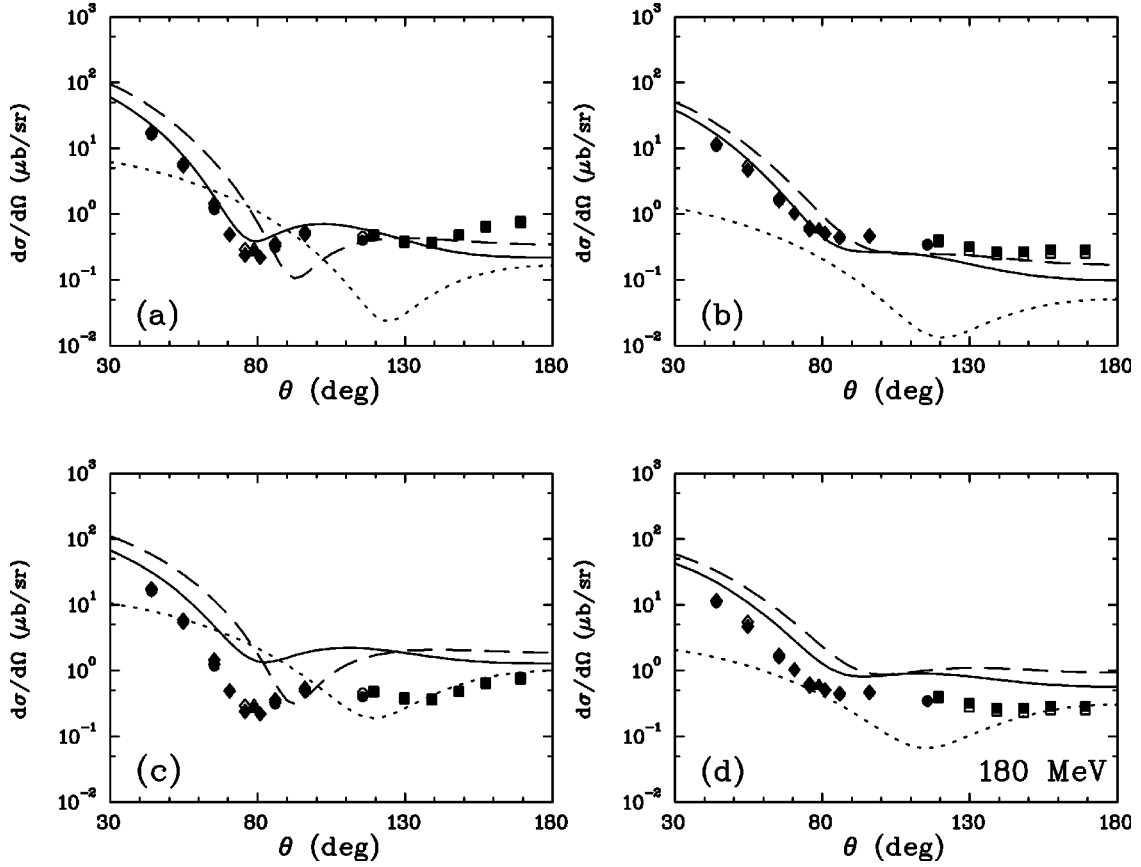


FIG. 3. Differential cross sections for $\pi^{\pm 3}\text{H}/^3\text{He}$ elastic scattering for $T_{\pi}=180$ MeV. The notation is the same as for Fig. 2.

vector \hat{s} , which is an integrative variable on the right-hand side of Eq. (14). We extract \hat{s} by introducing the operators $\hat{\Lambda}_{2,ij}$:

$$\hat{\Lambda}_2 = \sum_{i,j} \Lambda_{2,ij} \hat{s}_i \hat{s}_j. \quad (18)$$

Thus, the operator \hat{F}_2 can be expressed in the form

$$\hat{F}_2 = \sum_{i,j} f_{P_{33}}^2 \Lambda_{2,ij} I_{ij}, \quad (19)$$

where the tensor I_{ij} is expressed in the form

$$I_{ij} = J_1 \hat{\kappa}_i \hat{\kappa}_j + J_2 \delta_{ij}, \quad (20)$$

such that $\vec{\kappa} = (\vec{k}_1 + \vec{k}_2)/2$ and $\hat{\kappa} = \vec{\kappa}/|\vec{\kappa}|$. Here, the quantities J_1 and J_2 are complex functions which depend on the momentum of the incoming pion k_1 and the momentum transfer Δ (or on the scattering angle θ). They also depend on the WFs of the nuclei, which are given in Appendix B. Using Eq. (20) for the tensors I_{ij} , the amplitude \hat{F}_2 becomes

$$\hat{F}_2 = A_2 + iB_2 (\vec{\sigma} \cdot [\hat{\kappa}_1 \times \hat{\kappa}_2]). \quad (21)$$

We divide the contributions to A_2 and B_2 into double elastic scattering

$$\pi^- \rightarrow \pi^- \rightarrow \pi^-$$

(we will define this contribution via index “*ee*”) and double charge exchange

$$\pi^- \rightarrow \pi^0 \rightarrow \pi^-$$

(we will denote this contribution via index “*cc*”) in the functions A_2 and B_2 :

$$A_2 = A_2^{ee} + A_2^{cc}, \quad B_2 = B_2^{ee} + B_2^{cc}. \quad (22)$$

Then, we can present expressions for A_2 and B_2 in terms of the integrals J_1 and J_2 :

$$\begin{aligned} A_2^{cc} &= -\frac{1}{9} f_{P_{33}}^2 [(3+5z)J_1 + 12zJ_2], & B_2^{ee} &= \frac{4}{3} f_{P_{33}}^2 (J_1 + 2J_2), \\ A_2^{ee} &= \frac{1}{3} f_{P_{33}}^2 [(23+17z)J_1 + 28zJ_2], & B_2^{cc} &= -\frac{2}{9} f_{P_{33}}^2 \\ &\times (2J_1 + 3J_2) & \text{for } \pi^+{}^3\text{H}, \pi^-{}^3\text{H}, \\ A_2^{ee} &= \frac{1}{9} f_{P_{33}}^2 [(29+27z)J_1 + 52zJ_2], & B_2^{cc} &= -\frac{2}{9} f_{P_{33}}^2 \\ &\times (2J_1 + 5J_2) & \text{for } \pi^-{}^3\text{H}, \pi^+{}^3\text{H}. \end{aligned} \quad (23)$$

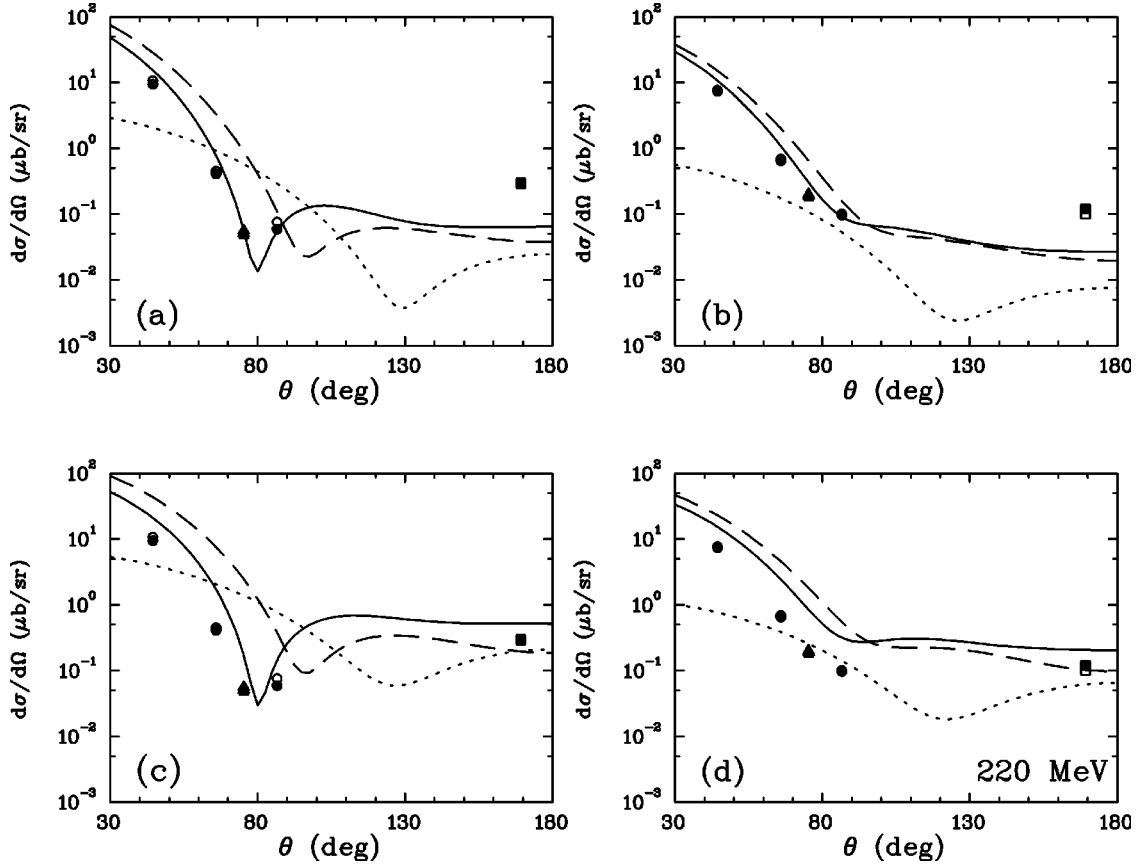


FIG. 4. Differential cross sections for $\pi^{\pm 3}\text{H}/^3\text{He}$ elastic scattering for $T_{\pi}=220$ MeV. The notation is the same as for Fig. 2.

The resulting double-scattering contributions to the differential cross sections are shown by the dotted curves in Figs. 2–5.

C. Nonresonant contributions

Although, the πN P -wave amplitude is dominant for the multiple scattering of pions in the nuclear medium in the energy range under consideration, the contribution of small nonresonant waves still can play an important role near $\theta \sim 90^\circ$ (the sharp minimum for single scattering). Thus, we limit ourselves to single scattering for nonresonant waves. In this limit, the πN amplitude (2) becomes

$$\hat{f}_{\pi N} = \sum_j f_j \cdot \hat{S}_j \cdot \hat{T}_j, \quad (24)$$

where

$$f_j = \frac{1}{2ik_{cm}} [e^{2i\delta_j(k)} - 1]$$

and \hat{S}_j and \hat{T}_j are the spin and isospin projection operators for the state j of the πN system. Limiting ourselves to S and P waves, the nonresonant πN $\delta_j(k)$ phases can be taken from a recent GW πN partial-wave analysis [25]. Therefore, we take into account two S and four P waves in our calculations. The projection operators are

$$\hat{S}_j = \hat{1} \quad (S_{11}, S_{31}),$$

$$\hat{S}_j = z - i(\vec{\sigma} \cdot \vec{n}) \quad (P_{11}, P_{31}),$$

$$\hat{S}_j = 2z + i(\vec{\sigma} \cdot \vec{n}) \quad (P_{13}, P_{33}),$$

$$\hat{T}_j = \frac{1}{3}(1 - \vec{t} \cdot \vec{\tau}) \quad (S_{11}, P_{11}, P_{13}),$$

$$\hat{T}_j = \frac{1}{3}(2 + \vec{t} \cdot \vec{\tau}) \quad (S_{31}, P_{31}, P_{33}), \quad (25)$$

where $\vec{n} = [\vec{k}_1 \times \vec{k}_2]$. We note that the procedure of taking into account nonresonant waves in the single-scattering approach is analogous to the resonant contribution taken into account and discussed in Sec. III A. The final expressions for the non-spin-flip and spin-flip nonresonant amplitudes are

$$A_{non} = \left[\frac{2}{3}f_{S_{11}} + \frac{7}{3}f_{S_{31}} + \left(\frac{2}{3}f_{P_{11}} + \frac{7}{3}f_{P_{31}} + \frac{4}{3}f_{P_{13}} \right) z \right] F(\Delta),$$

$$B_{non} = \frac{1}{3}(2f_{P_{13}} - f_{P_{31}} - 2f_{P_{11}})F(\Delta)$$

for $\pi^+ ^3\text{He}$ and $\pi^- ^3\text{H}$,

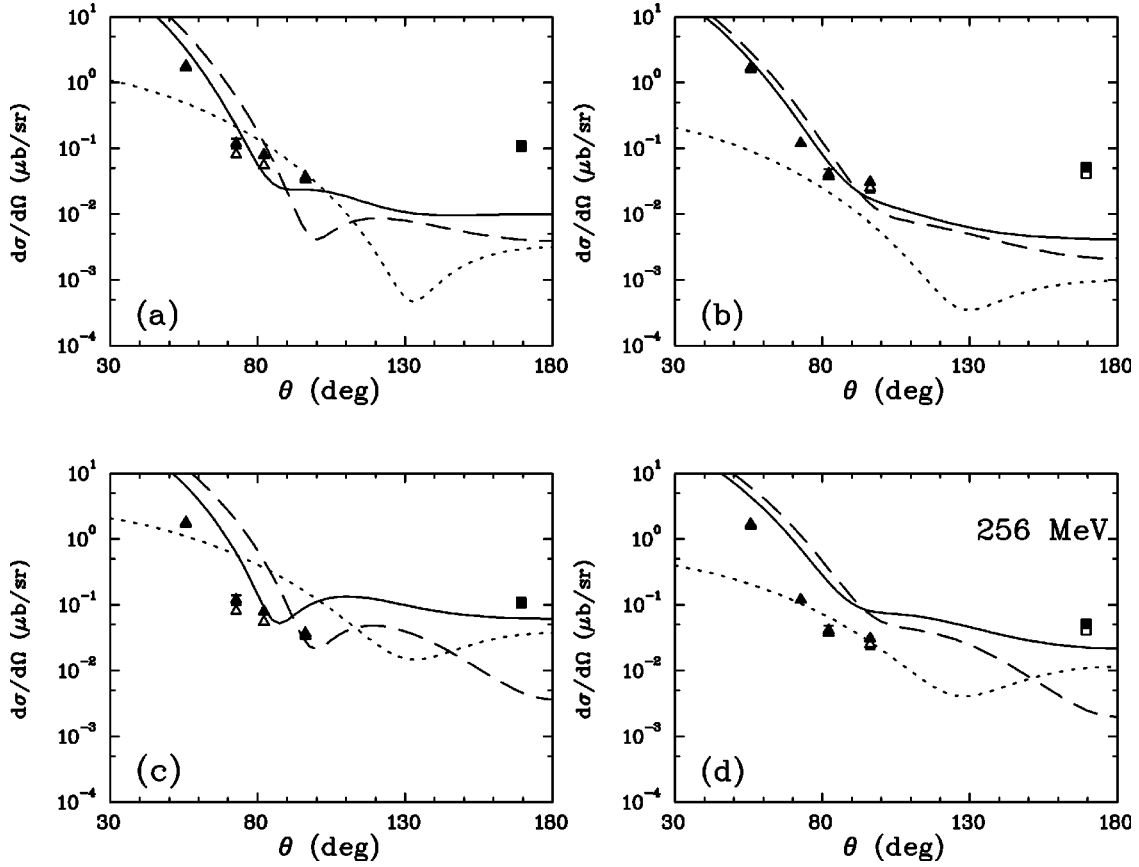


FIG. 5. Differential cross sections for $\pi^{\pm 3}\text{H}^3\text{He}$ elastic scattering for $T_{\pi}=256$ MeV. The notation is the same as for Fig. 2.

$$A_{non} = \left[\frac{4}{3}f_{S_{11}} + \frac{5}{3}f_{S_{31}} + \left(\frac{4}{3}f_{P_{11}} + \frac{5}{3}f_{P_{31}} + \frac{8}{3}f_{P_{13}} \right) z \right] F(\Delta),$$

$$B_{non} = -f_{P_{31}} F(\Delta) \quad \text{for } \pi^{-3}\text{He} \text{ and } \pi^{+3}\text{H}. \quad (26)$$

The nonresonant contribution for the total amplitude $\hat{F} = \hat{F}_1 + \hat{F}_2$ [see Eq. (27) below] is small and numerical values are taken from the analysis [25]. It is expressed by the substitutions

$$A \rightarrow A + A_{non}, \quad B \rightarrow B + B_{non}.$$

The nonresonant amplitudes are taken into account in the calculations of the ratios (1) presented in Sec. V.

D. Total amplitude and differential cross section

The expression for the sum of the single- and double-scattering amplitudes can be expressed in a form similar to Eq. (21):

$$\hat{F} = A + iB \quad (\vec{\sigma} \cdot [\hat{k}_1 \times \hat{k}_2]), \quad (27)$$

where the functions A and B represent the contributions of single and double scattering, e.g., $A = A_1 + A_2$ and $B = B_1 + B_2$. The amplitudes A_1 and B_1 are determined by Eqs.

(9)–(11) and (26), A_2 and B_2 by Eqs. (22) and (23). In terms of the functions A and B , the differential cross section in the unpolarized case has the form

$$\frac{d\sigma}{d\Omega} = \frac{1}{2} \text{Tr}\{\hat{F}^+ \hat{F}\} = |A|^2 + |B|^2 \sin^2 \theta. \quad (28)$$

The combined single- and double-scattering contributions, with interference taken into account, are depicted by the solid curves in Figs. 2–5. It can be seen that the model approach we use qualitatively agrees with the data. For forward scattering, $\theta \sim 30^\circ - 60^\circ$, WF (7) reproduces the cross sections systematically better than WF (8). At larger scattering angles, the results for WF (7) [WF (8)] lie below (above) the experimental data, and the cross-section minimum is shifted to a smaller angle ($\theta \sim 80^\circ$), in agreement with the experimental data. The key point to be made, however, is that the gentle maximum at $\theta \sim 110^\circ - 120^\circ$ arises from the interference between single and double scattering. It is also seen that the moderation of the rise in the cross sections for backward scattering reflects the contribution of double scattering, which is most pronounced near $\theta \sim 180^\circ$.

We point out that the description of hadron-nuclear scattering in the backward hemisphere is a very complicated multibody problem that requires detailed information about the wave function of the nucleus and the reaction mechanism. For example, the five-component WF used in Ref. [14] to describe the $\pi^{\pm 3}\text{He}$ elastic cross sections at T_{π}

=200 MeV is superior to WF (7). However, the goal of our study is the description and understanding of CSV effects, and these effects do not depend strongly on the details of the WF at small distances. For this reason, we prefer to use the simpler S -shell versions of the nuclear WFs (7) and (8).

IV. CHARGE-SYMMETRY VIOLATION EFFECTS

There are three principal sources of the violation of charge symmetry for π^\pm scattering from light nuclei in the Δ_{33} region:

- (i) the Coulomb interaction between the charged pions and the nuclei—the external Coulomb effect,
- (ii) the mass splitting of the different charge states of the Δ_{33} -isobar, and
- (iii) the difference between the WFs of ${}^3\text{H}$ and ${}^3\text{He}$ due to the additional Coulomb repulsion between the two protons in the ${}^3\text{He}$ nucleus—the internal Coulomb effect.

We now discuss how we take these effects into account in our calculation of the elastic scattering of charged pions from the $A=3$ nuclei.

A. External Coulomb effect

As was shown in Sec. II, experimental data for the ratios (1) [7–10] were taken outside the Coulomb cone, $\theta \gtrsim 30^\circ$. In this angular range, the Coulomb amplitude is a smooth function of the scattering angle θ . Here, we take into account the Coulomb interaction in a nonrelativistic approach, neglecting the interaction between the photon and the magnetic moment of the nucleus. Thus, the Coulomb amplitude of the pion-nucleus interaction in terms of the Coulomb phase may be written as

$$A_C = - \frac{Z_\pi Z_A e^2}{2k_{\text{c.m.}} \sin^2 \frac{\theta}{2}} \frac{\omega m_A}{m_A + \omega} \times \exp \left[- \frac{2iZ_\pi Z_A e^2}{k_{\text{c.m.}}} \frac{\omega m_A}{m_A + \omega} \ln \left(\sin \frac{\theta}{2} \right) \right] F_\pi(\vec{\Delta}) F(\vec{\Delta}), \quad (29)$$

where $e^2 \approx 1/137$, Z_π and Z_A are the charges of the pion and the nucleus, respectively, ω is the pion c.m. energy, m_A is the mass of the nucleus, $F(\vec{\Delta})$ is the form factor of the nucleus defined by Eq. (A4), and $F_\pi(\vec{\Delta})$ is the pion charge form factor that is used in the standard parametrization of Ref. [26]. In calculating the ratios (1), we use the amplitude A_C of Eq. (29) in combination with the non-spin-flip amplitude A of the strong interaction of Eq. (27) by the substitution $A \rightarrow A + A_C$.

B. $\Delta_{33}(1232)$ -mass splitting

The influence of the Δ_{33} -mass splitting on the differential cross section for πd elastic scattering was discussed in Ref. [5], where the single-scattering approximation with allow-

ance for the different charge states of the $\Delta_{33}(1232)$ was used. In this approximation, the CSV effect proves to be independent of the scattering angle, with a value proportional to $\delta m_\Delta / \Gamma_\Delta$. Nearly the same approach was used for the ${}^3\text{H}/{}^3\text{He}$ case in Ref. [7].

We denote the different charge states of the Δ_{33} via the index $i=1-4$ for the Δ^{++} , Δ^+ , Δ^0 , and Δ^- , respectively. The mass w_i ($i=1-4$), corresponding to the isobar i , is calculated according to a formula from Ref. [17] [p. 109, Eq. (4.18)], following Ref. [27]:

$$w_i = a - bI_i + cI_i^2, \quad (30)$$

where I_i is the third component of isospin for the i th term from the Δ_{33} multiplet. Using the average resonance mass value from the Particle Data Group [28], $\bar{w} = 1232$ MeV, $b = 1.38$ MeV from Ref. [17], and

$$w_3 - w_1 = m_{\Delta^0} - m_{\Delta^{++}} \approx 2.5 \text{ MeV}$$

from Ref. [28], we get

$$a \approx 1231.8 \text{ MeV}, \quad c = 0.13 \text{ MeV}.$$

The scalar amplitude for πN scattering [see Eq. (2)] for each charge state i is defined as

$$f_{P_{33}} \rightarrow f_i = \frac{1}{2ik_{\text{c.m.}}} [e^{2i\delta_i(k)} - 1]. \quad (31)$$

The phases δ_i are defined relative to the resonance phase $\delta_{P_{33}}$,

$$\delta_i = \delta_{P_{33}} - 2 \frac{\delta w_i}{\Gamma_\Delta} \sin^2 \delta_{P_{33}}, \quad (32)$$

where $\delta w_i = w_i - \bar{w}$. The resonance phase $\delta_{P_{33}}$ is taken from Ref. [25]. In Eq. (32), we neglect the energy dependence of the width Γ_Δ because $\delta w_i / \Gamma_\Delta \ll 1$; in our calculations we use $\Gamma_\Delta = 120$ MeV. Using this definition of f_i for the πN scattering amplitudes in Eq. (31), we obtain the following expressions for the single pion-nucleus scattering amplitudes:

$$A_1 = (2f_1 + \frac{1}{3}f_2)2zF(\vec{\Delta}), \quad B_1 = \frac{1}{3}f_2F(\vec{\Delta}) \quad \text{for } \pi^+{}^3\text{He}, \quad (33)$$

$$A_1 = (f_1 + \frac{2}{3}f_2)2zF(\vec{\Delta}), \quad B_1 = f_1F(\vec{\Delta}) \quad \text{for } \pi^+{}^3\text{H}. \quad (34)$$

Substituting $f_1 \rightarrow f_4$ and $f_2 \rightarrow f_3$, the amplitudes A_1 and B_1 in Eqs. (33) and (34) are transformed to the amplitudes for the isomirror reactions $\pi^-{}^3\text{H}$ and $\pi^-{}^3\text{He}$.

For the double-scattering pion-nucleus amplitudes, we obtain

$$A_2^{cc} = - \frac{1}{9} f_2^2 [(3 + 5z)J_1 + 12zJ_2],$$

$$B_2^{ee} = \frac{4}{3} f_1 f_2 (J_1 + 2J_2) \quad \text{for } \pi^+{}^3\text{He}, \pi^+{}^3\text{H} \quad (35)$$

instead of Eq. (23). The other amplitudes for $\pi^{+3}\text{He}$ and $\pi^{+3}\text{H}$ elastic scattering are different:

$$\begin{aligned}
 A_2^{ee} &= \frac{4}{3}f_1f_2[2(1+z)J_1+4zJ_2] \\
 &\quad + f_1^2[(5+3z)J_1+4zJ_2] \quad \text{for } \pi^{+3}\text{He}, \\
 A_2^{ee} &= \frac{4}{3}f_1f_2[2(1+z)J_1+4zJ_2] \\
 &\quad + \frac{1}{9}f_2^2[(5+3z)J_1+4zJ_2] \quad \text{for } \pi^{+3}\text{H}, \\
 B_2^{cc} &= -\frac{2}{9}f_2^2(2J_1+3J_2) \quad \text{for } \pi^{+3}\text{He}, \\
 B_2^{cc} &= -\frac{2}{3}f_2^2(2J_1+5J_2) \quad \text{for } \pi^{+3}\text{H}. \quad (36)
 \end{aligned}$$

The amplitudes A_2 and B_2 of Eqs. (35) and (36) are also transformed to their isomirror reaction amplitudes, i.e., $\pi^{+3}\text{He} \rightarrow \pi^{-3}\text{H}$ and $\pi^{+3}\text{H} \rightarrow \pi^{-3}\text{He}$, by substituting $f_1 \rightarrow f_4$ and $f_2 \rightarrow f_3$. We do not include any difference for the different charge states in the nonresonant amplitudes A_{non} and B_{non} .

C. Internal Coulomb effect

The difference in the structure of the WFs of ${}^3\text{H}$ and ${}^3\text{He}$ is related not only to the electromagnetic interaction, but also to the part of the strong interaction which violates isospin. In the strong-interaction sector, there are terms that violate isospin directly [2]. Isospin violation inside nuclei can relate to both nucleon and quark degrees of freedom. In terms of quark degrees of freedom, isospin violation relates to the mass difference of the u and d quarks. At present, there is no quantitatively good estimate of isospin violation due to the strong interaction for the $A=3$ nuclei.

If we assume that the strong interaction conserves isospin, then the main reason for the difference in the structure of the WFs of ${}^3\text{H}$ and ${}^3\text{He}$ is the additional Coulomb repulsion between the two protons in ${}^3\text{He}$, which is not present for ${}^3\text{H}$. If there were no Coulomb interaction between these two protons (i.e., if the WFs of ${}^3\text{H}$ and ${}^3\text{He}$ were isotopically symmetric), the neutron distribution for ${}^3\text{He}$ (the ‘‘odd’’ neutron) would be the same as the proton distribution for ${}^3\text{He}$ (the ‘‘odd’’ proton), and the proton distribution for ${}^3\text{He}$ (the ‘‘even’’ protons) would be the same as the neutron distribution for ${}^3\text{H}$ (the ‘‘even’’ neutrons). However, the proton distributions for ${}^3\text{H}$ and ${}^3\text{He}$ can still be different and, as a consequence, so can the charge form factors of ${}^3\text{H}$ and ${}^3\text{He}$.

If, however, isospin is violated for ${}^3\text{H}$ and ${}^3\text{He}$, the even- and odd-nucleon distributions can also be different. In Ref. [15], the difference between these distributions has been formulated in terms of nonzero parameters δ_e and δ_o , where

$$\delta_e = r_e^n - r_e^p, \quad \delta_o = r_o^n - r_o^p.$$

Here $r_{e,o}^{n,p}$ is the neutron (n) or proton (p) radius for the even (e) or odd (o) nucleons. As was shown in Ref. [15], the superratio R at $T_\pi=180$ MeV is very sensitive to δ_e and δ_o ; a reasonable description of R versus scattering angle has been obtained for $\delta_e = -0.030 \pm 0.008$ fm and $\delta_o = 0.035 \pm 0.007$ fm. These differences between r_e^n and r_e^p or between r_o^n and r_o^p due to isospin violation result in additional changes in the charge radii and form factors of ${}^3\text{H}$ and ${}^3\text{He}$.

We vary the parameters of the WFs (7) and (8) to introduce such differences. For WF (7), we follow the recipe suggested in Ref. [14]: we fix the slope b for ${}^3\text{H}$ at 1.65 fm and vary the slope for ${}^3\text{He}$ to obtain the best description of the data for the ratios r_1 and r_2 . An analogous procedure is followed for WF (8), using parameters for the WF for ${}^3\text{He}$ suggested in Ref. [22] (see Sec. III). Then, for the WF of ${}^3\text{H}$, we use three different variations of the WF: (i) a variation of the slope α_1 , (ii) a variation of the slope α_2 , and (iii) a variation of both slopes α_1 and α_2 , which are proportional to each other: $\alpha_1 \rightarrow c\alpha_1$ and $\alpha_2 \rightarrow c\alpha_2$.

Although this variation of the parameters of WFs (7) and (8) cannot be compared directly with the refined procedure used in Ref. [15], this way of taking into account the internal Coulomb interaction allows us to take the $\Delta_{33}(1232)$ -mass splitting into account, which was not done in Ref. [15]. Therefore, the quantities δ_e and δ_o obtained from the experimental data can differ from the values obtained in Ref. [15].

V. COMPARISON WITH THE EXPERIMENTAL DATA

A. Excluding the internal Coulomb effect

The results of our calculations for the ratios r_1 , r_2 , and the superratio R which take into account the external Coulomb interaction and the Δ_{33} -mass splitting but exclude the internal Coulomb effect are shown in Figs. 6–9, as the dotted curves for single scattering and the dashed curves for both single and double scattering. There are no free parameters associated with these results. The main purpose of Figs. 6–9 (as for Figs. 2–5) is to show that the inclusion of double scattering is essential to be able to follow the trend of the data in the non-spin-flip-dip region. As is seen in these figures, there is qualitative agreement between the results of our calculations and the data for $T_\pi=180, 220, \text{ and } 256$ MeV. Also, in contrast with the case for the differential cross section (see Figs. 2–5), there is little sensitivity to the WF here. For $T_\pi=180$ MeV, the ratio r_1 is reproduced very well for both WFs (7) and (8), but the peaks near $\theta=80^\circ$ in the ratio r_2 and superratio R are reproduced better by WF (7). At the same time, the description of r_2 and R in the backward direction is not good for either WF. Figure 7 shows that even taking into account single scattering and the external Coulomb interaction cannot reproduce the experimental data there. But overall, Figs. 7–9 show that taking into account the Δ_{33} -mass splitting consistently with both the single- and double-scattering contributions reproduces the main structures of the angular distribution and to shows that we do not require a detailed knowledge of the nuclear WF.

We note here that the data for r_2 and R for $T_\pi=142$ MeV are not reproduced by our model approach. Ap-

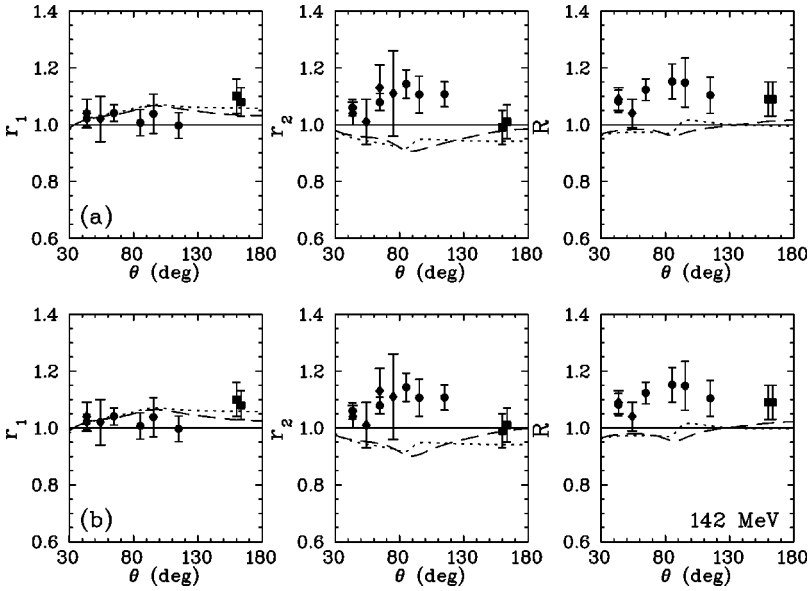


FIG. 6. The ratios r_1 and r_2 and the super-ratio R for $T_\pi=142$ MeV. Experimental data are from Refs. [7] (diamonds), [8] (circles), [9] (triangles), and [10] (squares). Only the Δ_{33} -mass splitting and external Coulomb contributions are taken into account. The full calculations take into account both single and double scattering, and are shown by the dashed curves. The results for single scattering alone are shown by the dotted curves. Plotted are the results for (a) WF (7) and (b) WF (8).

parently, some other mechanism must play a role at this energy. We return to this problem below.

B. Including the internal coulomb effect

We now describe the CSV effects by taking into account the internal Coulomb interaction as well. The procedure for variation of the WFs is described above. For this case, we vary a single free parameter to obtain the best fit. Again, we fit r_1 and r_2 only, since the superratio $R (=r_1 \cdot r_2)$ is not an independent quantity. The best-fit results for this approach and for both WFs (7) and (8) are shown in Figs. 10–13 by the solid curves. By comparison, the results without the internal Coulomb interaction (from Figs. 6–9) are shown by the dashed curves. Both free parameters α_1 and α_2 have been varied simultaneously, following our prescription (iii) of Sec. IV. The results of varying either α_1 or α_2 independently are very similar, as listed in Table I. In this table, the

best-fit results obtained by variations of the radii of the nuclei and corresponding χ^2 values are listed as well.

In Fig. 11, we see that our calculations reproduce all the ratios r_1 , r_2 , and R for $T_\pi=180$ MeV rather well over the entire angular range. In fact, we reproduce the superratio R for $40^\circ \leq \theta \leq 110^\circ$ much as did Gibbs and Gibson [15]. Taking into account the difference in the WFs of ${}^3\text{H}$ and ${}^3\text{He}$ results in a much better reproduction both of the quantity R at $\theta \sim 80^\circ$ and the scattering at backward angles. Thus, taking into account the internal Coulomb interaction provides a substantial improvement in χ^2 compared with the case where only the external Coulomb interaction and the Δ_{33} -mass splitting are included.

Finally, we consider the description of the data for $T_\pi=220$ and 256 MeV to be qualitatively satisfactory, while the description of the data for $T_\pi=142$ MeV is not. Consider the situation for $T_\pi=220$ MeV, shown in Fig. 12. Our theoretic-

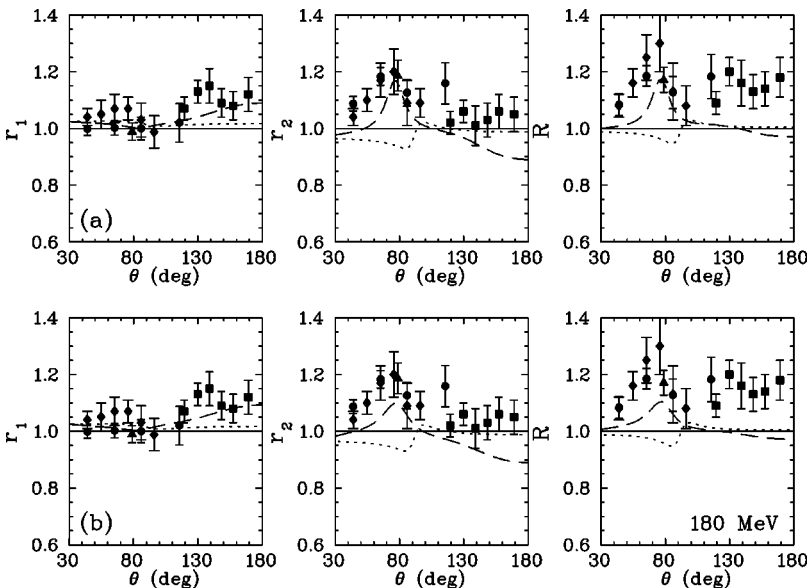


FIG. 7. The ratios r_1 and r_2 and the super-ratio R for $T_\pi=180$ MeV. The notation is the same as for Fig. 6.

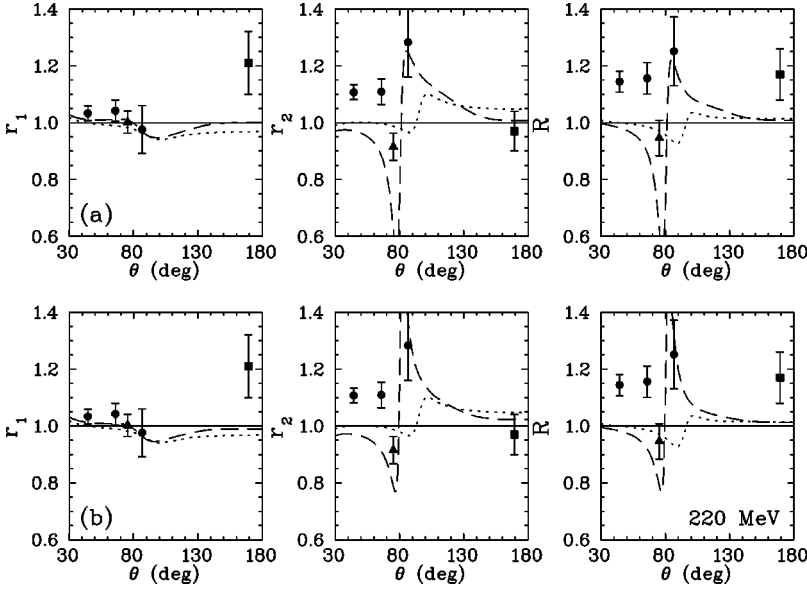


FIG. 8. The ratios r_1 and r_2 and the super-ratio R for $T_\pi=220$ MeV. The notation is the same as for Fig. 6.

cal curves reproduce the sharp dip-bump angular dependence of the ratios r_2 and R remarkably well. At $T_\pi=256$ MeV, shown in Fig. 13, we predict a more gradual dip-bump angular dependence, which also agrees with the experimental data. At the same time, our theoretical curves do not reproduce the data for $T_\pi=142$ MeV, shown in Fig. 10, even though the angular dependence is much smoother. We note, however, that the amount of experimental data for $T_\pi=220$ and 256 MeV is significantly less than for $T_\pi=142$ and especially for 180 MeV. Evaluation of the $T_\pi=142$ MeV data may require an additional mechanism to reproduce the behavior of the data.³

VI. ADDITIONAL REMARKS

A. Δ_{33} -mass splitting and total cross sections

We have seen that one of the principal sources of CSV is the Δ_{33} -mass splitting. The difference in the total $\pi^\pm d$ cross sections is determined by the Δ_{33} -mass splitting [17]. Here we calculate this effect for the ratios r_{1t} and r_{2t} for the *total* cross sections of $\pi^\pm {}^3\text{H}/{}^3\text{He}$ scattering, defined as

$$r_{1t} = \frac{\sigma^{tot}(\pi^+ {}^3\text{H})}{\sigma^{tot}(\pi^- {}^3\text{He})}, \quad r_{2t} = \frac{\sigma^{tot}(\pi^- {}^3\text{H})}{\sigma^{tot}(\pi^+ {}^3\text{He})}.$$

We predict a considerably larger CSV effect for the three-nucleon system than for the deuteron, as shown in Fig. 14. Moreover, the crossover of r_{1t} and r_{2t} at the peak of the Δ_{33} , for either of the WFs used, establishes a unique signature for this effect.

The high sensitivity of CSV to the N^* -mass splitting (within multiplets) allows us to suggest the use of these ratios as a method to determine the mass splitting in heavy

N^* 's and Δ^* 's. We think that this method would be preferable to the traditional πN partial-wave analysis for baryon spectroscopy.

B. Accuracy of calculations

In our theoretical approach to single and double scattering, we neglect the Fermi motion of the nucleons inside the nucleus. The amplitude of the πN scattering is extracted from an integral over incident pion energies that are on shell. We also neglect the recoil of the nucleons in the Green's function G_π of Eq. (14) for the double-scattering amplitude. We call this approach the “fixed-centers approximation.” Then, we observe that when only certain corrections are taken into account, we obtain worse agreement with the experimental data (see Ref. [20] for details).

Since the fixed-centers approximation gives results that are close to the data, there must be cancellations of the main corrections to leading order. These cancellations for hadron-deuteron scattering have been discussed in detail in previous work. The cancellation of nonadiabatic corrections within the Glauber approach for differential cross sections at high energies was shown in Ref. [29]. In the πd scattering-length calculations, the cancellation of off-shell and recoil corrections was discussed in Ref. [30]. The cancellation of nonadiabatic corrections for πd elastic scattering was found in the range of the Δ_{33} resonance in Ref. [31]. Apparently, the analogous cancellation of corrections holds as well for the $A=3$ nuclei. Therefore, the use of only a few of the corrections to the fixed-centers approximation can result in worse agreement with the data than when all the corrections are ignored. Inclusion of all the corrections (including the so-called binding corrections) is a rather complicated task and is not a goal of our present study.

For example, we limit ourselves to the consideration of single- and double-scattering terms, and this approach allows us to take into account the leading terms of the amplitude of the pion-nuclear interaction at energies and scattering angles where we can qualitatively reproduce the shape of the distri-

³In the most advanced study [15], the authors considered only the case for $T_\pi=180$ MeV. On the other hand, the calculation of Ref. [14] does not reproduce the CSV effect for 142 MeV either.

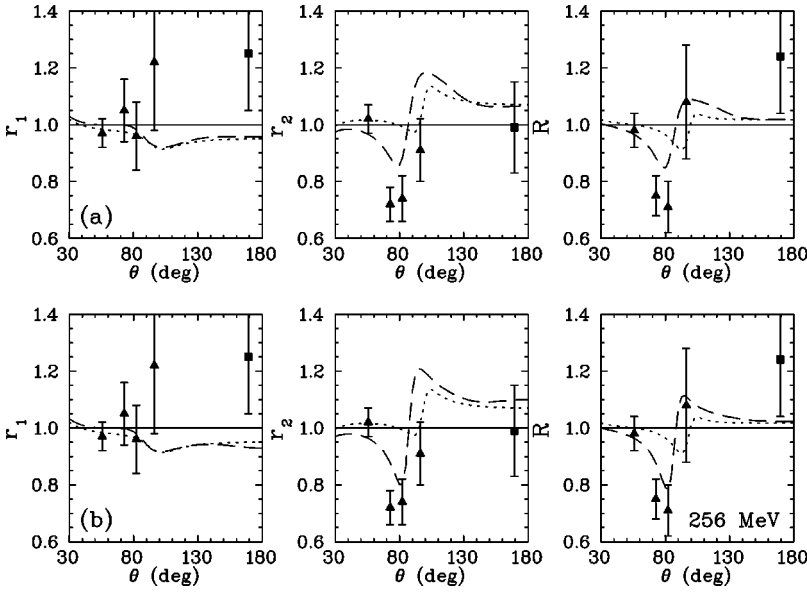


FIG. 9. The ratios r_1 and r_2 and the super-ratio R for $T_\pi=256$ MeV. The notation is the same as for Fig. 6.

bution of the differential cross sections. Triple-scattering contributions to the differential cross sections can smooth the angular shape, but they are more difficult to calculate and cannot be simplified by the transformation of the integrals J_1 and J_2 discussed in Appendix B.

C. Pion absorption

At small scattering angles, $\theta \sim 30^\circ - 60^\circ$, there is reasonable agreement between our theoretical approach and the experimental data for $T_\pi = 180$ MeV and above, but for $T_\pi = 142$ MeV the experimental cross sections are smaller than the results of our model calculations for both WFs used (Figs. 2–5). But because for modest scattering angles the range of momentum transfer is small ($Q \leq 150$ MeV/ c), our use of the simple WFs (7) and (8) is reasonable. We therefore infer that the suppression of the cross section for $T_\pi = 142$ MeV results from absorption, which is absent in our model approach for the amplitude of the πA interaction. Usually, the absorption on a nucleus is due to the reaction $\pi(NN) \rightarrow NN$, where (NN) is a pair of correlated nucleons. But the total cross section of the $\pi d \rightarrow NN$ reaction has its maximum at $T_\pi = 140$ MeV, and the absorption cross section is somewhat suppressed at $T_\pi = 180$ MeV [32]. However, $T_\pi = 180$ MeV corresponds to the maximum of the total $\pi^\pm d$ cross section, as shown in Fig. 15. The pion absorption cross section for ${}^3\text{He}$, measured at PSI [33], also peaks at $T_\pi = 140 - 150$ MeV, as shown in Fig. 15 as well. Therefore, if absorption were responsible for the suppression of the scattering cross sections at small scattering angles for $T_\pi = 142$ MeV, then this effect would be considerably smaller for $T_\pi = 180$ MeV, where our fit to the data is much better.

D. CSV in $\pi^\pm {}^4\text{He}$ elastic scattering

Data for the elastic $\pi^\pm {}^4\text{He}$ differential cross sections have been obtained at LAMPF for T_π below, at, and above the Δ_{33} resonance [34]. The spin-flip amplitudes for elastic $\pi^\pm {}^4\text{He}$ in the single-scattering approximation do not contribute to

the Δ_{33} resonance. Preliminary analysis of the charge asymmetry for $T_\pi = 180$ MeV shows a statistically significant effect in A_π , of the order of 10% at scattering angles $\theta \sim 70^\circ - 90^\circ$ [35]. The size of A_π for $T_\pi \leq 180$ MeV and the possible influence of absorption there are still unknown.

Because of the larger role played by pion absorption on heavier nuclei, CSV is expected to be suppressed relative to the three- and four-body nuclei. If present, CSV in heavier nuclei probably depends more on their geometrical properties than on the Δ_{33} -mass splitting.

VII. SUMMARY

We have performed theoretical calculations for the simple ratios r_1 and r_2 and the superratio R for elastic $\pi^\pm {}^3\text{H}/{}^3\text{He}$ scattering, for $T_\pi = 142, 180, 220,$ and 256 MeV and over a broad angular range. We have found reasonable agreement between the results of our calculations and the experimental data, shown in Fig. 1 of the associated paper by Briscoe *et al.* [10], over most of the range of the data.

Our calculations were done with an approach utilizing the sum of the single- and double-scattering πN contributions, as indicated in Fig. 1. We took into account three sources of CSV—the Δ_{33} -mass splitting and the external and internal Coulomb interactions. We used S -shell WFs for ${}^3\text{H}$ and ${}^3\text{He}$. This approach enabled us to use simple analytical expressions for the double-scattering contribution to pion-nuclear scattering, taking into account all spin and isospin amplitudes. We used two different radial WFs for the $A = 3$ nuclei:

(i) A simple Gaussian distribution [Eq. (7)] with the slope describing the charge densities of ${}^3\text{H}$ and ${}^3\text{He}$ obtained from electron scattering [21,36–38]. We used the WF of Ref. [14].

(ii) A sum of two Gaussian WFs [Eq. (8)], as used in Ref. [22] for the description of the differential cross sections of the reaction ${}^4\text{He}(p,d){}^3\text{He}$. This WF reproduces the minimum of the ${}^3\text{He}$ charge form factor at $Q = 670$ MeV/ c , but is larger than the experimental data at smaller momentum transfer.

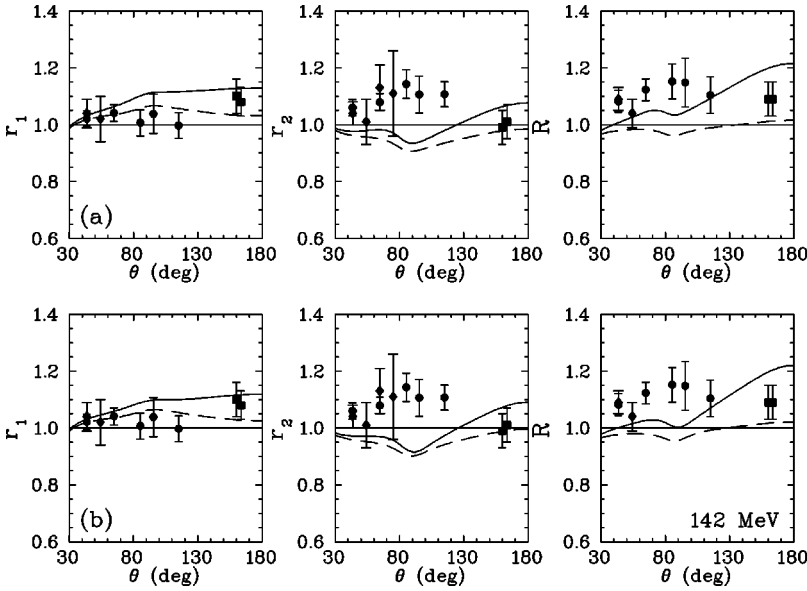


FIG. 10. The ratios r_1 and r_2 and the super-ratio R for $T_\pi=142$ MeV. The notation for the experimental data is the same as for Fig. 6. The Δ_{33} -mass splitting with external (and internal) Coulomb contributions are shown by the dashed (solid) curves. Plotted are the results for (a) WF (7) and (b) WF (8). Version (iii) of the variation of the WFs is shown, as described in Sec. IV.

The calculated cross sections, shown in Figs. 2–5, agree qualitatively with the experimental data. For $T_\pi=180$ MeV, the theoretical curves have minima at $\theta \sim 140^\circ-150^\circ$ and reproduce the gradual growth of the cross sections as θ approaches 180° , indicating the importance of the inclusion of double scattering for the differential cross sections. Of course, the absolute cross sections are very sensitive to the WF, and are not reproduced well by the simple S-shell approach used here.

The main goal of our study is the calculation of the CSV effects for $\pi^{\pm 3}\text{H}/^3\text{He}$ differential cross sections in terms of the observables r_1 , r_2 , and R . No free parameters are used in our approach when taking into account the Δ_{33} -mass splitting and the external Coulomb interaction. Figures 7–9 show that these factors alone account qualitatively for major features of the data. These figures also show that there is little sensitivity to the choice of the wave function.

Figures 11–13 show that when the internal Coulomb ef-

fect is included as well, there is reasonable agreement between our theoretical calculations and the experimental data. The best agreement is found for $T_\pi=180$ MeV (at the peak of the Δ_{33} resonance). Both the Δ_{33} -mass splitting and the internal Coulomb interaction are important for the reproduction of the shape of the angular distribution, both near the non-spin-flip dip at $\theta \sim 80^\circ$ and at large scattering angles. Although the influence of the internal Coulomb interaction on CSV has been shown before [15], our investigation shows that including the Δ_{33} -mass splitting results in a still better description of the effect of CSV, as it should: the Δ_{33} -mass splitting exists, so its effects should not be ignored. We also predict the simple mirror ratios for the total cross sections, as shown in Fig. 14.

Finally, however, as seen from Figs. 6 and 10, our calculations do not reproduce the data for $T_\pi=142$ MeV. Although we tried to take into account a number of different approaches beyond the framework of our model (more accu-

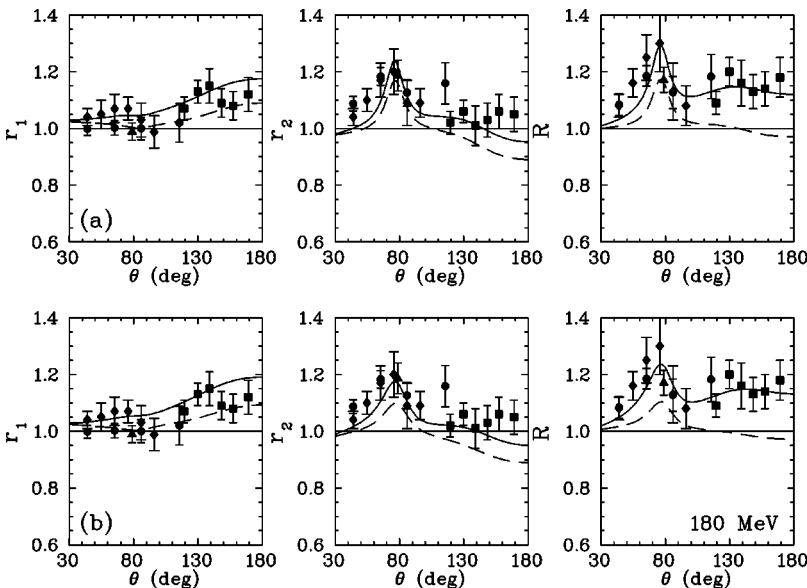


FIG. 11. The ratios r_1 and r_2 and the super-ratio R for $T_\pi=180$ MeV. The notation is the same as for Fig. 10.

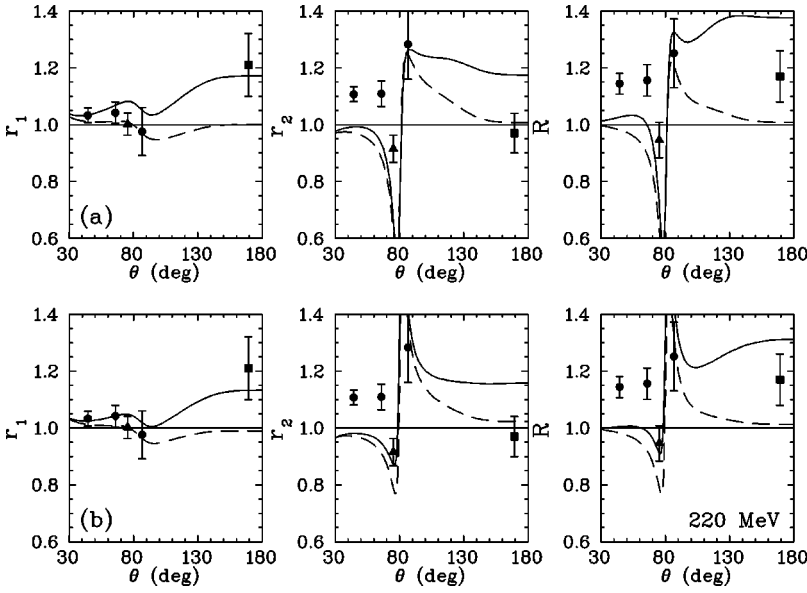


FIG. 12. The ratios r_1 and r_2 and the super-ratio R for $T_\pi=220$ MeV. The notation is the same as for Fig. 10.

rate amplitudes for single and double scattering and Fermi motion, etc.), we were not able to improve the agreement for $T_\pi=142$ MeV. Therefore, the question of the nature of the effect of CSV for $T_\pi=142$ MeV remains open. Perhaps there is an additional mechanism at $T_\pi=142$ MeV which does not manifest itself at higher energies; Fig. 15 shows that quite possibly, pion absorption plays a major role.

ACKNOWLEDGMENTS

The authors acknowledge very useful communications with B. V. Geshkenbein, S. S. Kamalov, and C. L. Morris. This work was supported in part by the U.S. Department of Energy under Grant Nos. DE-FG02-95ER40901 and DE-FG02-99ER41110 and by the Russian Grant for Basic Research Nos. 98-02-17618 and N 00-15-96562. A.K. acknowledges the hospitality extended by the Center for Nuclear Studies of The George Washington University. I.S. acknowledges partial support from Jefferson Lab, by the Southeast-

ern Universities Research Association under DOE Contract No. DE-AC05-84ER40150.

APPENDIX A: THE CHARGE FORM FACTOR $F(\vec{\Delta})$

Let us introduce relative coordinates of the nucleons $\vec{\rho}_i = \vec{r}_j - \vec{r}_k$ and $\vec{R}_i = \frac{1}{2}(\vec{r}_j + \vec{r}_k) - \vec{r}_i$ instead of \vec{r}_i . In terms of these new variables, the function ψ of Eq. (5) yields

$$\psi(\vec{r}_1, \vec{r}_2, \vec{r}_3) \equiv \psi \left[\sum_{m=1}^3 (\vec{r}_i - \vec{R}_0)^2 \right] = \psi \left(\frac{\vec{\rho}_i^2}{2} + \frac{2}{3} \vec{R}_i^2 \right) = \psi(\vec{\rho}, \vec{R}). \quad (\text{A1})$$

This function ψ does not depend on the selection of a basis $i(jk)$. The Fourier transformation of the function ψ is defined by

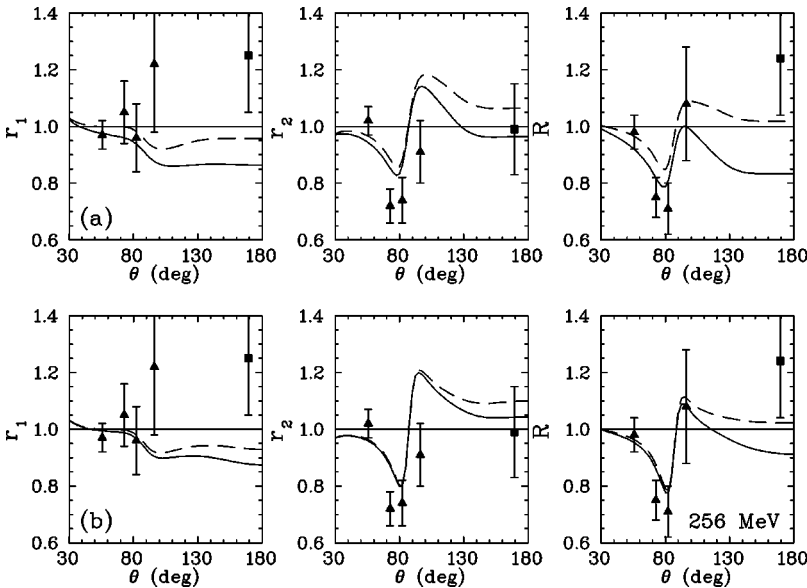


FIG. 13. The ratios r_1 and r_2 and the super-ratio R for $T_\pi=256$ MeV. The notation is the same as for Fig. 10.

TABLE I. Best-fit results for the ratios r_1 and r_2 from variation of the ${}^3\text{H}$ and ${}^3\text{He}$ WFs. The slope b has been varied for the WF (7) (Ref. [14]). Cases (i)–(iii) of variations of the WF (8) (Ref. [22]) have been discussed in the text. Differences in the mean-square charge radii $\delta r = r({}^3\text{He}) - r({}^3\text{H})$ and χ^2/df are listed in columns 5 and 6. The last column shows χ^2/df when the internal Coulomb interaction is not taken into account.

T_π (MeV)	WF (Refs.)	Varied parameter		δr (fm)	χ^2/df	χ^2/df ($\delta r=0$)
142	[14]	b		0.015	3.90	4.87
	[22]	α_1	(i)	0.017	4.15	
		α_2	(ii)	0.010	4.44	5.06
180	[14]	b		0.012	1.68	2.88
	[22]	α_1	(i)	0.017	1.60	
		α_2	(ii)	0.014	1.65	3.05
220	[14]	b		0.016	1.61	
	[22]	α_1 and α_2	(iii)	0.016	1.61	10.5
			α_1	(i)	0.016	5.37
256	[22]	α_2	(ii)	0.011	5.37	6.74
		α_1 and α_2	(iii)	0.014	5.36	
	[14]	b		-0.010	2.26	2.43
256	[22]	α_1	(i)	-0.006	2.29	
		α_2	(ii)	0	2.37	2.37
		α_1 and α_2	(iii)	-0.003	2.35	

$$\varphi(\vec{q}, \vec{Q}) = \int d^3\vec{\rho} d^3\vec{R} \psi(\vec{\rho}, \vec{R}) \exp(-i\vec{q} \cdot \vec{r} - i\vec{Q} \cdot \vec{R}), \quad (\text{A2})$$

where $\vec{q} = \vec{q}_i = (\vec{p}_j - \vec{p}_k)/2$ and $\vec{Q} = \vec{Q}_i = (\vec{\rho}_j + \vec{p}_k - 2\vec{p}_i)/3$ are relative momenta and $(\vec{p}_i, \vec{p}_j, \vec{p}_k)$ are the momenta of the nucleons of the nucleus. For the WF (8), $\varphi(\vec{q}, \vec{Q})$ has the form

$$\varphi(\vec{q}, \vec{Q}) = N \left(\frac{\pi}{\sqrt{12}} \right) \sum_m \frac{D_m}{\alpha_m^3} \exp\left(-\frac{q^2}{\alpha_m} - \frac{3Q^2}{4\alpha_m}\right), \quad (\text{A3})$$

where

$$N^{-2} = \frac{9}{2} (\pi\sqrt{12})^3 \sum_{m,n} \frac{D_m D_n}{(\alpha_m + \alpha_n)^2}.$$

The charge form factor for elastic scattering is defined by

$$F(\vec{\Delta}) = \frac{9}{2} \int \frac{d\vec{q}}{(2\pi)^3} \frac{d\vec{Q}}{(2\pi)^3} \varphi\left(\vec{q}, \vec{Q} - \frac{2}{3}\vec{\Delta}\right) \varphi(\vec{q}, \vec{Q}), \quad (\text{A4})$$

$$F(0) = 1.$$

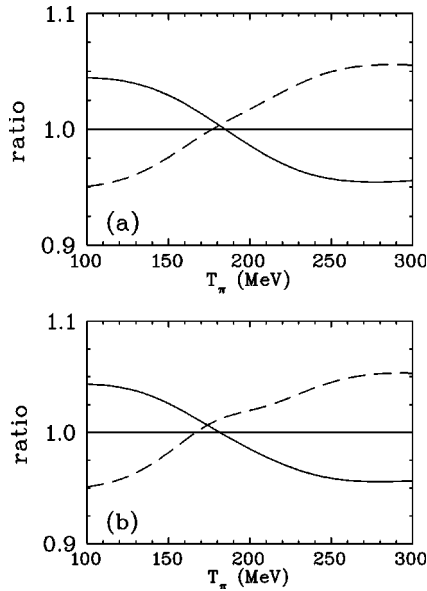


FIG. 14. Predictions for the ratios r_{1t} (solid), and r_{2t} (dashed) for the total $\pi^\pm {}^3\text{H}/{}^3\text{He}$ cross sections. Calculations were done for single and double scattering with the Δ_{33} -mass splitting. The Coulomb interactions are not taken into account. Plotted are the results for (a) WF (7) and (b) WF (8).

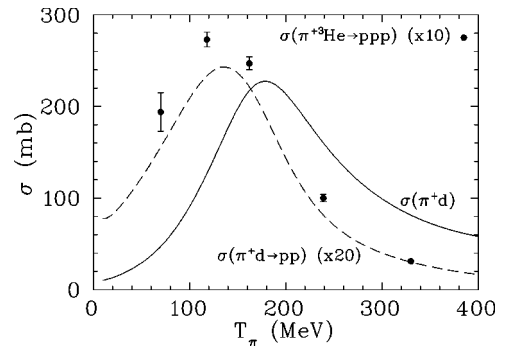


FIG. 15. Total π^+ cross sections. Plotted are cross sections for π^+d (solid) and $\pi^+d \rightarrow pp$ (multiplied by a factor of 20) (dashed) from a recent combined fit of the pp and πd elastic scattering with the $\pi^+d \rightarrow pp$ data [32]. The $\pi^3\text{He}$ absorption data (multiplied by a factor of 10) are from [33] (filled circles); it can be seen that they peak near $T_\pi = 140$ MeV.

An analytical expression for the form factor (A4) corresponding to the WF (8) is

$$F(\vec{\Delta}) = N_0^{-1} \sum_{m,n} \frac{D_m D_n}{(\alpha_m + \alpha_n)^3} \exp\left[-\frac{\Delta^2}{3(\alpha_m + \alpha_n)}\right], \quad (\text{A5})$$

where

$$N_0 = \sum_{m,n} \frac{D_m D_n}{(\alpha_m + \alpha_n)^3}. \quad (\text{A6})$$

APPENDIX B:

THE TENSOR I_{ij} AND THE FUNCTIONS J_1 AND J_2

The expression for the tensor I_{ij} in terms of the wave function $\varphi(\vec{q}, \vec{Q})$ (A2) is

$$I_{ij} = 4\pi \int \frac{d^3 \vec{q}}{(2\pi)^3} \frac{d^3 \vec{Q}}{(2\pi)^3} \frac{d^3 \vec{Q}'}{(2\pi)^3} \times \varphi(\vec{q}', \vec{Q}') \varphi(\vec{q}, \vec{Q}) \frac{\hat{s}_i \hat{s}_j}{k_1^2 - s^2 - i0}. \quad (\text{B1})$$

This integral is suitable for calculations in coordinate space. To do this, we follow a transformation first used in Ref. [31]:

$$\frac{\hat{s}_i \hat{s}_j}{k_1^2 - s^2 - i0} = \frac{1}{4\pi} \int \exp(i\vec{s} \cdot \vec{r}) H_{ij}(\vec{r}) d\vec{r}, \quad (\text{B2})$$

where

$$H_{ij}(\vec{r}) = h_1(r) \hat{r}_i \hat{r}_j + h_2(r) \delta_{ij}$$

and

$$h_1(r) = \frac{e^{ikr}}{r} + \frac{3ie^{ikr}}{kr^2} - \frac{3e^{ikr}}{k^2 r^3} + \frac{3}{k^2 r^3},$$

$$h_2(r) = \frac{e^{ikr}}{k^2 r^3} - \frac{1}{k^2 r^3} - \frac{ie^{ikr}}{kr^2}.$$

Then, using Eq. (B2) and the coordinate expression for the wave function (A1), we get the expression for the tensor I_{ij} :

$$I_{ij} = \frac{2}{9} \int d^3 \vec{\rho} d^3 \vec{r} \psi^2(\vec{\rho}, \vec{R}) H_{ij}(\vec{r}) \exp\left[i\left(\vec{k}_1 - \frac{\vec{\Delta}}{3}\right) \cdot \vec{r} + i\frac{\vec{\Delta} \cdot \vec{\rho}}{3}\right], \quad (\text{B3})$$

where $\vec{R} = \vec{r} + \frac{1}{2}\vec{\rho}$. If the WF $\psi(\vec{\rho}, \vec{R})$ is expressed as a sum of several Gaussians, the integral (B3) can be represented in the form of expression (20). Then the integrals J_1 and J_2 are transformed into one-dimensional integrals. For the WF (8), they have the form

$$J_{1,2} = \frac{2}{9} N^2 \sum_{m,n} D_m D_n \left(\frac{3\pi}{a_{mn}}\right)^{1/2} \exp\left(-\frac{\Delta^2}{12a_{mn}}\right) F_{1,2}(a_{mn}, \theta),$$

where

$$F_1(a, \theta) = \pi \int_0^\infty r^2 \exp\left(\frac{ar^2}{4}\right) (3E_2 - E_0) h_1(r) dr,$$

$$F_2(a, \theta) = \pi \int_0^\infty r^2 \exp\left(\frac{ar^2}{4}\right) \times [(E_0 - E_2) h_1(r) + 2E_0 h_2(r)] dr,$$

$$E_n = \int_{-1}^1 \exp(i\xi r z) z^n dz, \quad (\text{B4})$$

$\xi = k \cos \theta/2$, $\Delta = 2k \sin \Delta/2$, and N is given by Eq. (A3). In the case of WF (7), the expressions for the integrals $J_{1,2}$ are computed easily from Eq. (B4).

-
- [1] G.A. Miller, B.M.K. Nefkens, and I. Slaus, *Phys. Rep.* **194**, 1 (1990).
- [2] S. Weinberg, in *Chiral Dynamics: Theory and Experiment*, edited by A. M. Bernstein and B. R. Holstein (Springer, New York, 1994), p. 3.
- [3] U.-G. Meissner, in *Proceedings of 9th International Symposium on Meson-Nucleon Physics and the Structure of the Nucleon, Washington, DC, 2001*, edited by H. Haberzettl and W. J. Briscoe [*πN Newslett.* **16**, 1 (2001)].
- [4] A. Gashi, E. Matsinos, G.C. Oades, G. Rasche, and W.S. Woolcock, *nucl-th/0009081*.
- [5] T.G. Masterson, J.J. Kraushaar, R.J. Peterson, R.S. Raymond, R.A. Ristinen, R.L. Boudrie, E.F. Gibson, and A.W. Thomas, *Phys. Rev. C* **26**, 2091 (1982).
- [6] V.V. Baru, A.E. Kudryavtsev, V.E. Tarasov, W.J. Briscoe, K.S. Dhuga, and I.I. Strakovsky, *Phys. Rev. C* **62**, 044003 (2000).
- [7] B.M.K. Nefkens, W.J. Briscoe, A.D. Eichon, D.H. Fitzgerald, A. Mokhtari, J.A. Wightman, and M.E. Sadler, *Phys. Rev. C* **41**, 2770 (1990).
- [8] C. Pillai, D.B. Barlow, B.L. Berman, W.J. Briscoe, A. Mokhtari, B.M.K. Nefkens, and M.E. Sadler, *Phys. Rev. C* **43**, 1838 (1991).
- [9] K.S. Dhuga, B.L. Berman, W.J. Briscoe, R.W. Caress, S.K. Matthews, D.B. Barlow, B.M.K. Nefkens, C. Pillai, J.W. Price, S.J. Greene, I. Slaus, and I. Supek, *Phys. Rev. C* **54**, 2823 (1996).
- [10] W.J. Briscoe, B.L. Berman, R.W. Carter, K.S. Dhuga, S.K. Matthews, N.-J. Nicholas, S.J. Greene, B.M.K. Nefkens, J.W. Price, L.D. Isenhower, M.E. Sadler, I. Slaus, and I. Supek, *Phys. Rev. C* **66**, 054006 (2002), preceding paper.
- [11] B.L. Berman, G.C. Anderson, W.J. Briscoe, A. Mokhtari, A.M. Petrov, M.E. Sadler, D.B. Barlow, B.M.K. Nefkens, and C.

- Pillai, Phys. Rev. C **51**, 1882 (1995).
- [12] S.K. Matthews, W.J. Briscoe, C. Bennhold, B.L. Berman, R.W. Caress, K.S. Dhuga, S.N. Dragic, S.S. Kamalov, N.J. Nicholas, M.F. Taragin, L. Tiator, S.J. Greene, D.B. Barlow, B.M.K. Nefkens, C. Pillai, J.W. Price, L.D. Isenhower, M.E. Sadler, I. Slaus, and I. Supek, Phys. Rev. C **51**, 2534 (1995).
- [13] Kr.T. Kim, Y.E. Kim, and R.H. Landau, Phys. Rev. C **36**, 2155 (1987).
- [14] S.S. Kamalov, L. Tiator, and C. Bennhold, Phys. Rev. C **47**, 941 (1993).
- [15] W.R. Gibbs and B.F. Gibson, Phys. Rev. C **43**, 1012 (1991).
- [16] E. Pedroni, K. Gabathuler, J.J. Domingo, W. Hirt, P. Schwaller, J. Arvieux, C.H.Q. Ingram, P. Gretillat, J. Piffaretti, N.W. Tanner, and C. Wilkin, Nucl. Phys. **A300**, 321 (1978).
- [17] T. Ericson and W. Weise, *Pions and Nuclei* (Clarendon, Oxford, 1988).
- [18] G.R. Smith *et al.*, Phys. Rev. C **38**, 240 (1988).
- [19] S. K. Matthews, Ph.D. thesis, The George Washington University, 1993.
- [20] W.J. Briscoe, A.E. Kudryavtsev, I.I. Strakovsky, and V.E. Tarasov, Yad. Fiz. **64**, 1507 (2001) [Phys. At. Nucl. **64**, 1430 (2001)].
- [21] F.-P. Juster, S. Auffret, J.-M. Cavedon, J.-C. Clemens, B. Frois, D. Goutte, M. Huet, P. Leconte, J. Martino, Y. Mizuno, X.-H. Phan, S. Platchkov, S. Williamson, and I. Sick, Phys. Rev. Lett. **55**, 2261 (1985).
- [22] A. Foursat, E. Lyovshin, and K. Sailer, Nucl. Phys. **A392**, 399 (1983).
- [23] R.H. Landau, Comput. Phys. Commun. **28**, 109 (1982).
- [24] S.L. Collier and W.R. Gibbs, Phys. Rev. C **59**, 1290 (1999).
- [25] R.A. Arndt, R.L. Workman, I.I. Strakovsky, and M.M. Pavan, nucl-th/9807087.
- [26] S.R. Amendolia *et al.*, Nucl. Phys. **B277**, 168 (1986).
- [27] S. Weinberg and S.B. Treiman, Phys. Rev. **116**, 465 (1959).
- [28] Particle Data Group, D.E. Groom *et al.*, Eur. Phys. J. C **15**, 1 (2000).
- [29] V.M. Kolybasov and L.A. Kondratyuk, Phys. Lett. **39B**, 439 (1972).
- [30] G. Fäldt, Phys. Scr., **16**, 81 (1977); V.M. Kolybasov and V.G. Ksenzov, Zh. Éksp. Teor. Fiz. **71**, 13 (1976) [Sov. Phys. JETP **71**, 13 (1976)]; V.G. Ksenzov, Yad. Fiz. **28**, 1249 (1978) [Sov. Phys. JETP **28**, 644 (1978)]; O.D. Dalkarov, V.M. Kolybasov, and V.G. Ksenzov, Nucl. Phys. **A397**, 498 (1983); V.V. Baru and A.E. Kudryavtsev, Yad. Fiz. **60**, 1620 (1997) [Phys. At. Nucl. **60**, 1475 (1997)].
- [31] V.M. Kolybasov and A.E. Kudryavtsev, Yad. Fiz. **17**, 32 (1973) [Sov. J. Nucl. Phys. **17**, 42 (1973)].
- [32] C.H. Oh, R.A. Arndt, I.I. Strakovsky, and R.L. Workman, Phys. Rev. C **56**, 635 (1997).
- [33] A. Lehmann *et al.*, Phys. Rev. C **55**, 2931 (1997).
- [34] B. Brinkmüller *et al.*, Phys. Rev. C **44**, 2031 (1991).
- [35] C. L. Morris (private communication).
- [36] J.S. McCarthy, I. Sick, and R.R. Whitney, Phys. Rev. C **15**, 1396 (1977).
- [37] D. Beck *et al.*, Phys. Rev. Lett. **59**, 1537 (1987).
- [38] A. Amroun, V. Breton, J.-M. Cavedon, B. Frois, D. Goutte, J. Martino, X.-H. Phan, S.K. Platchkov, I. Sick, and S. Williamson, Phys. Rev. Lett. **69**, 253 (1992).